

# On the role and origin of nonthermal electrons in hot accretion flows

Andrzej Niedźwiecki, Agnieszka Stępnik

*Department of Astrophysics, University of Łódź, Pomorska 149/153, 90-236 Łódź, Poland*

niedzwiecki@uni.lodz.pl, agajer@o2.pl

Fu-Guo Xie

*Key Laboratory for Research in Galaxies and Cosmology, Shanghai Astronomical Observatory, Chinese Academy of Sciences, 80 Nandan Road, Shanghai 200030, China*

fgxie@shao.ac.cn

## ABSTRACT

We study the X-ray spectra of tenuous, two-temperature accretion flows using a model involving an exact, Monte Carlo computation of the global Comptonization effect as well as general relativistic description of both the flow structure and radiative processes. In our previous work we found that in flows surrounding supermassive black holes, thermal synchrotron radiation is not capable of providing a sufficient seed photons flux to explain the X-ray spectral indices as well as the cut-off energies measured in several best-studied AGNs. In this work we complete the model by including seed photons provided by nonthermal synchrotron radiation and we find that it allows to reconcile the hot flow model with the AGN data. We take into account two possible sources of nonthermal electrons. First, we consider  $e^\pm$  produced by charged-pions decay, which should be always present in the innermost part of a two-temperature flow due to proton-proton interactions. We find that for a weak heating of thermal electrons (small  $\delta$ ) the synchrotron emission of pion-decay  $e^\pm$  is much stronger than the thermal synchrotron emission in the considered range of bolometric luminosities,  $L \sim (10^{-4} - 10^{-2})L_{\text{Edd}}$ . The small- $\delta$  model including hadronic effects in general agrees with the AGN data, except for the case of a slowly rotating black hole and a thermal distribution of protons. For large  $\delta$ , the pion-decay  $e^\pm$  have a negligible effect and then in this model we consider nonthermal electrons produced by direct acceleration. We find an approximate agreement with the AGN data for the fraction of the heating power of electrons which is used for the nonthermal acceleration  $\eta \sim 0.1$ . However, for constant  $\eta$  and  $\delta$ , the model predicts a positive correlation of the X-ray spectral index with the Eddington ratio, and hence a fine tuning of  $\eta$  and/or  $\delta$  with the accretion rate is required to explain the negative correlation observed at low luminosities. We note a significant difference between the dependence of plasma parameters,  $T_e$  and  $\tau$ , on the Eddington ratio that is predicted by the large- and small- $\delta$  models. This may be the key property allowing for estimation of the value of  $\delta$ . However, a precise measurement of the spectral cut-off is required and we note that differences between results available in literature are similar in magnitude to the difference between the model predictions. In flows surrounding stellar-mass black holes, the synchrotron emission of pion-decay  $e^\pm$  exceeds the thermal synchrotron only above  $\sim 0.01L_{\text{Edd}}$ . Furthermore, in such flows the nonthermal synchrotron radiation is emitted at energies  $\gtrsim 1$  keV, and therefore the Compton cooling is less efficient than in flows surrounding supermassive black holes. This may explain spectral differences between AGNs and black-hole transients around  $\sim 0.01 L_{\text{Edd}}$  (the latter being typically much harder).

*Subject headings:* accretion, accretion discs – black hole physics – galaxies: active

## 1. Introduction

Optically thin, hot accretion flows are widely considered as a relevant accretion mode below  $\sim 0.01L_{\text{Edd}}$  in black-hole binaries as well as in AGNs, and the X-ray radiation - typically dominating the radiative output at low luminosities - is most likely produced by thermal Comptonization in the inner parts of such flows (see reviews in Zdziarski & Gierliński 2004, Done et al. 2007, Yuan & Narayan 2014, Poutanen & Veledina 2014). In our previous work (Niedźwiecki et al. 2014, hereafter N14) we considered the standard version of hot-flow models, with seed photons for Comptonization provided mainly by thermal synchrotron radiation. We found that such a model roughly agrees with observations of several well studied black hole transients for bolometric luminosities between  $\sim 10^{-4}L_{\text{Edd}}$  and  $10^{-2}L_{\text{Edd}}$ . For a small sample of well studied AGNs, observed in the same luminosity range, we found a strong disagreement with the model predictions; the predicted spectra are much harder than observed and their cut-off energies are too high.

This clearly indicates that in hot flows around supermassive black holes, thermal synchrotron emission is not capable of providing the required flux of seed photons for thermal Comptonization, which is the main cooling process at such luminosities. In this paper we consider extension of the model, taking into account the presence of nonthermal electrons and their nonthermal synchrotron emission. The presence of such a non-thermal component can significantly increase the efficiency of Compton cooling (see Wardziński & Zdziarski 2001, Veledina et al. 2011); while thermal synchrotron is strongly self-absorbed, the non-thermal synchrotron is emitted at higher frequencies and subject to weaker self-absorption, therefore, it is a much more efficient source of seed photons. See also Poutanen & Veledina (2014) for arguments supporting the presence of nonthermal electrons in hot flows.

Our model essentially follows the original formulation of advection dominated accretion flow (ADAF) model (e.g. Narayan & Yi 1995). Relatively weak Coulomb coupling between protons and electrons in a tenuous plasma results in a two-temperature structure, which is a key property of ADAF solutions, as such flows are supported by

proton pressure. In the innermost part of the flow, the hot protons have energies above the threshold for pion production. Therefore, relativistic  $e^\pm$  from charged-pions decay should be always present in ADAFs. Their nonthermal synchrotron emission was previously studied by Mahadevan (1999, hereafter M99) for the radio emission of Sgr A\*, however, it has never been self-consistently implemented as a source of seed photons in models of high-energy emission.

Nonthermal particles may be also directly produced by nonthermal acceleration, e.g. by magnetic reconnection induced by the magneto-rotational instability (cf. Riquelme et al. 2012). We take it into account by considering both a nonthermal distribution of protons in hadronic models and the presence of a nonthermal population of electrons not related with the  $\pi^\pm$ -decay rate. In the latter case the amount of nonthermal electrons is a free parameter (in contrast to the hadronic model); such models with simple descriptions of accretion flow (one-zone or approximate radial dependence) have been considered in the context of ADAF solutions e.g. by Malzac & Belmont (2009), Veledina et al. (2011).

## 2. Model

We apply the model developed in our recent works, see Niedźwiecki et al. (2012, hereafter N12) and N14, except for the source of seed photons, which includes nonthermal synchrotron radiation, whereas in the previous studies we took into account only thermal synchrotron emission (and bremsstrahlung, which is negligible for accretion rates considered in our works). We consider a black hole, characterized by its mass,  $M$ , and angular momentum,  $J$ , surrounded by a geometrically thick accretion flow with an accretion rate,  $\dot{M}$ . We define the following dimensionless parameters:  $r = R/R_g$ ,  $a = J/(cR_gM)$ ,  $\dot{m} = \dot{M}/\dot{M}_{\text{Edd}}$ , where  $\dot{M}_{\text{Edd}} = L_{\text{Edd}}/c^2$ ,  $R_g = GM/c^2$  is the gravitational radius and  $L_{\text{Edd}} \equiv 4\pi GMm_p c/\sigma_T$  is the Eddington luminosity. We assume that the density distribution is given by  $n(R, z) = n(R, 0) \exp(-z^2/2H^2)$ , where  $H$  is the height scale at  $R$  and  $z = R \cos \theta$ . We define the vertical optical depth as  $\tau = H\sigma_T n$ .

We assume the viscosity parameter,  $\alpha = 0.3$ , and the ratio of the gas pressure (electron and ion)

to the magnetic pressure,  $\beta$ . The fraction of the dissipated energy which heats directly electrons is denoted by  $\delta$ .

We find the global hydrodynamical solution of the general relativistic (GR) structure equations following Manmoto (2000) with modifications described in N12. Most importantly, we use the global Compton cooling rate computed using a GR Monte Carlo (MC) method, whereas in similar studies local approximations are usually applied (see Yuan et al. 2009, Xie et al. 2010, N12 and N14 for discussion of related inaccuracies). We find the self-consistent electron temperature distribution,  $T_e(r)$ , by iterating between the solutions of the electron energy equation and the GR MC Comptonization simulations until we find mutually consistent solutions. This procedure involves assumption that other parameters of the flow (density, proton temperature, height scale, velocity field) are not affected by changes in  $T_e$ , which limits the maximum luminosity of the flow to  $\sim 0.01 L_{\text{Edd}}$  (at larger luminosities the Coulomb cooling of protons becomes important and the flow is characterized by a dramatic dependence on even small changes of  $T_e$ ). The minimum luminosity of flows which can be studied with our current model,  $\sim 10^{-4} L_{\text{Edd}}$ , is given by the requirement that the energy balance for electrons is determined by radiative cooling (rather than advection).

The total luminosity detected far away from the flow is denoted by  $L$  and the luminosity detected in the 2-10 keV range by  $L_{2-10}$ .

The thermalization as well as cooling time-scales for protons are much longer than the accretion time-scale,  $\simeq R/|v^r|$ , so the distribution of protons is determined by heating/acceleration processes which are poorly understood. We then consider two limiting cases by assuming that (i) all protons have a Maxwellian distribution; (ii) a small fraction of protons has a power-law distribution,  $n_{\text{pl}}(\gamma) \propto \gamma^{-s_p}$ , and the remaining protons are cold. These two models are identical to models T and N, respectively, in Niedźwiecki et al. (2013, hereafter N13); in particular, the fraction of protons with the power-law distribution is given by equation (7) in N13. We also consider (only in Fig. 3b) a hybrid model, with half of the energy stored in the thermal population of protons and another half in the nonthermal (power-law) population. For each distribution function of protons,

their energy density at each  $r$  is equal to that obtained from the hydrodynamic solution. Note that in the hydrodynamic solutions we always assume a thermal distribution, however, for a nonthermal distribution the flow structure should not change significantly (cf. Kimura et al. 2014).

In the computation of the rate of  $e^\pm$  production by charged-pion decay and their nonthermal synchrotron radiation we follow M99, except for interactions between power-law protons which are taken into account in our model and neglected by M99; the simplification applied by M99 underestimates the power in proton-proton interaction products by a factor of  $\sim 2$  (see N13). We also used the GALPROP code (Moskalenko & Strong 1998) to test our computations of the production and decay of  $\pi^\pm$ .

For all distributions of protons, the energy spectrum of the produced  $e^\pm$  has a maximum at  $\sim 35$  MeV. For a thermal distribution, it declines exponentially at higher energies. For a power-law proton distribution, it is the power-law at high energies with the same slope as the proton distribution, i.e. the injection index of electrons,  $s_{\text{inj}}$ , equals  $s_p$ . For the range of parameters considered in this work, at  $r < 1000$  for all relevant electron energies, the synchrotron cooling time is much shorter than the accretion time, so in all hadronic models the steady state electron distribution is  $N(\gamma) \propto \gamma^{-2}$  for Lorentz factors  $\gamma \lesssim 70$ . For  $\gamma \gg 70$ ,  $N(\gamma) \propto \gamma^{-(s_p+1)}$  for the power-law distribution of protons, whereas  $N(\gamma)$  decreases exponentially for the thermal distribution of protons (cf. figure 1 in M99). We have also checked that the Compton cooling time of nonthermal electrons is longer than the synchrotron cooling time, so the steady state distribution is determined by the synchrotron cooling rate.

The time-scale to establish pair equilibrium (with  $e^\pm$  creation by pion decay balanced by pair annihilation) is of the order of the accretion time scale (and much longer than the cooling time scale of nonthermal  $e^\pm$ ). Therefore, an approximate pair equilibrium should be established in the flow. In all models the equilibrium density of pion-decay  $e^\pm$  is at least by 2 orders of magnitude lower than the density of the ionization electrons, so the hadronic  $e^\pm$  contribute negligibly to the optical depth.

In models considering directly accelerated elec-

trons we assume that a fraction  $\eta$  of the total power heating electrons,  $\delta Q_{\text{diss}}$  (where  $Q_{\text{diss}}(r)$  is the total power dissipated at  $r$ ), is used for direct acceleration of electrons, so at each radius the power used for the acceleration is  $\eta\delta Q_{\text{diss}}$ , while  $(1 - \eta)\delta Q_{\text{diss}}$  is used for heating of thermal electrons.

In summary, we consider several versions of the hot-flow model. The purely thermal version, for which the thermal synchrotron radiation is the only source of seed photons, is referred to as the *standard* model **S**. The extension of the model, taking into account additional seed photons from nonthermal synchrotron of relativistic  $e^\pm$  produced by  $\pi^\pm$ -decay, is referred to as the *hadronic model* and depending on the assumed distribution function of protons it is denoted by **HT** (for thermal protons), **HN** (for power-law proton distribution) or **HH** (for hybrid distribution with equal energies in a thermal and power-law proton components). The model taking into account a *direct acceleration* of electrons is referred to as model **DA**. We consider model DA only for  $\delta = 0.5$ , for which hadronic processes have a negligible effect (see below), so we do not consider cases mixing strong effects of pion-decay and directly accelerated electrons. All results presented in this work for model HN or HH correspond to the proton power-law index  $s_p = 2.6$ .

### 3. Results

#### 3.1. Pion-decay electrons

Figs 1 and 2 illustrate crucial properties of the nonthermal synchrotron radiation produced by pion-decay  $e^\pm$ , its effect on the Comptonized radiation and the dependence on key parameters. Fig. 1a shows the spectral distribution of the synchrotron radiation, for  $M = 10 M_\odot$  and  $M = 2 \times 10^8 M_\odot$ . For these values of  $M$ , the magnetic field in the innermost part of the flow is  $B \sim (10^6 - 10^8)$  G and  $B \sim (10^2 - 10^4)$  G, respectively. In all hadronic models, regardless of the model parameters, the dominating contribution to the nonthermal synchrotron component is produced by electrons with  $\gamma_0 \sim 100$  and the nonthermal synchrotron spectrum has a maximum at  $\nu_{\text{max}} (\simeq \nu_c \gamma_0^2, \text{ where } \nu_c = eB/2\pi m_e c)$  which equals  $\nu_{\text{max}} \sim (10^{13} - 10^{16})$  Hz for  $M = 2 \times 10^8 M_\odot$  and  $\nu_{\text{max}} \sim (10^{17} - 10^{20})$  Hz for  $M = 10 M_\odot$ .

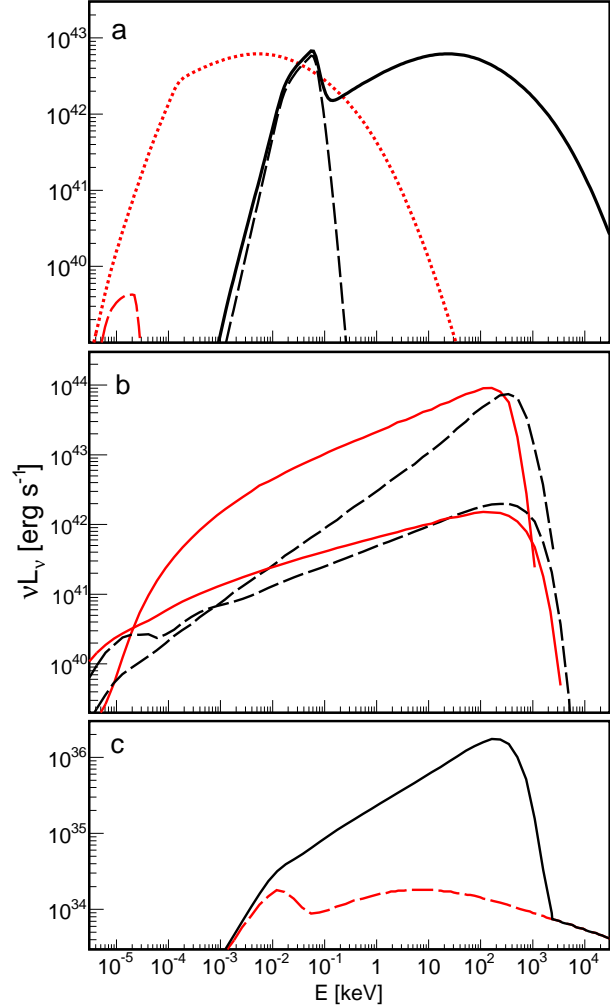


Fig. 1.— (a) *Rest-frame* spectra of the total synchrotron radiation for model HT with  $a = 0.95$ ,  $\beta = 1$ ,  $\delta = 10^{-3}$  and  $\dot{m} = 0.5$  are shown by the (red) dotted line for  $M = 2 \times 10^8 M_\odot$  and by the (black) solid line (scaled by  $2 \times 10^7$ ) for  $M = 10 M_\odot$ . Dashed lines show contribution from thermal synchrotron radiation. (b) (Red) solid lines show the *observed* spectra of synchrotron radiation and its thermal Comptonization for model HT with  $a = 0.95$ ,  $\beta = 1$ ,  $\delta = 10^{-3}$ ,  $M = 2 \times 10^8 M_\odot$ ; the (black) dashed lines are for model S with the same parameters. In both models  $\dot{m} = 0.1$  and  $0.5$  from bottom to top. (c) (Black) solid line shows the *observed* spectrum for model HN with  $a = 0.95$ ,  $\beta = 1$ ,  $\delta = 10^{-3}$ ,  $M = 10 M_\odot$  and  $\dot{m} = 0.5$ ; (red) dashed line shows the contribution of synchrotron radiation.

We use the synchrotron absorption coefficient (e.g. equation 1 in Ghisellini & Svensson 1991) to compute the self-absorption frequency,  $\nu_t$  (below which the flow is optically thick to absorption), in the hybrid electron distribution consisting of the thermal and the steady-state nonthermal components. We find (in agreement with M99) that the presence of pion-decay electrons has a small effect on  $\nu_t$ ; for  $M = 10 M_\odot$  it negligibly affects the value of  $\nu_t$  and for  $M = 2 \times 10^8 M_\odot$  it increases  $\nu_t$  by a factor of  $\sim 2$ . In all models the Lorentz factor of electrons radiating at  $\sim \nu_t$  is  $\gamma \sim 10$  so, with  $N(\gamma) \propto \gamma^{-2}$  at  $\gamma \ll \gamma_0$ , only a small fraction of the power injected in pion-decay electrons is emitted below  $\nu_t$  and most of the nonthermal emission is available as a seed photon input for Comptonization.

For  $M = 2 \times 10^8 M_\odot$ , Fig. 1b compares the spectra of the synchrotron emission and its thermal Comptonization observed by a distant observer in the hadronic and standard models with the same parameters. As we can see, the much stronger seed photon flux in the hadronic model gives much lower electron temperatures, which is reflected in a reduced cut-off energy and much softer X-ray spectra.

Fig. 1c shows the contribution of the synchrotron radiation to the *observed* spectrum for model HN with  $M = 10 M_\odot$ . Note that due to GR transfer effects the observed nonthermal synchrotron radiation has the maximum, in  $\nu F_\nu$ , at energies an order of magnitude lower than the rest-frame spectrum.

The high-energy part of the nonthermal synchrotron spectra depends on the proton distribution. In model HN it is a power-law with the photon spectral index  $\Gamma = 1 + s_p/2$ , as in Fig. 1c (where, for  $s_p = 2.6$ ,  $\Gamma = 2.3$ ). In model HT it decreases exponentially, as in Fig. 1a. However, this difference at high-energies does not affect the impact on electron temperature so, in particular, the same  $T_e$  is predicted by model HN and HT within large  $a$  (see below).

Fig. 2a shows the radial distribution of vertically integrated emissivities of thermal,  $Q_{\text{th},s}$ , and nonthermal,  $Q_{\text{nth},s}$ , synchrotron radiation. Figs 2bc show the ratio of the total nonthermal and thermal synchrotron emissivities,  $Q_{\text{nth},s,\text{tot}}$  and  $Q_{\text{th},s,\text{tot}}$ , computed by integrating  $Q_{\text{nth},s}$  and  $Q_{\text{th},s}$ , respectively, over  $r$ . Open symbols cor-

respond to  $Q_{\text{th},s,\text{tot}}$  in hadronic (or DA) models and full symbols to  $Q_{\text{th},s,\text{tot}}$  in model S; the difference between them illustrates the amount of the decrease of  $T_e$  due to the additional seed photons from nonthermal synchrotron. Note that the results of Wardziński & Zdziarski (2001) imply that  $Q_{\text{nth},s,\text{tot}}/Q_{\text{th},s,\text{tot}} \sim 10^5$  should correspond to the supermassive black-hole model, whereas our model gives much lower values. The difference is due to a small  $kT_e = 50$  keV assumed in Wardziński & Zdziarski and to a very strong sensitivity of  $Q_{\text{th},s}$  on  $T_e$ , with the increase of  $T_e$  by a factor of 2 corresponding to the increase of  $Q_{\text{th},s}$  by over an order of magnitude. Indeed, if we artificially set  $kT_e = 50$  keV in our models, we get  $Q_{\text{nth},s,\text{tot}}/Q_{\text{th},s,\text{tot}} \sim 10^5$ , however, the electron energy balance typically yields larger  $T_e$  at  $L/L_{\text{Edd}} \lesssim 0.01$ .

Below we briefly summarize the dependence on  $M$ ,  $\dot{m}$ ,  $a$ ,  $\delta$  and the proton distribution function.

*Heating of electrons.* For large  $\delta$ , the pion-decay  $e^\pm$  have insignificant effect and the hadronic models differ negligibly from corresponding model S, see stars in Fig. 2b. In these models,  $L$  is by an order of magnitude larger than in models with small  $\delta$  with the same  $\dot{m}$ , therefore, the rate of proton-proton interactions (which depends on density squared, i.e.  $\propto \dot{m}^2$ ) is by two orders of magnitude lower than in small- $\delta$  models with the same  $L$ . Below we focus on low- $\delta$  models.

*Black hole mass.* We find that in models with  $M = 10 M_\odot$  the presence of pion-decay  $e^\pm$  negligibly affects the electron temperature. Thermal synchrotron emissivity scales with  $M$  as  $Q_{\text{s},\text{th}} \sim M^{1/2}$  (Mahadevan 1997). Nonthermal synchrotron emissivity of  $\pi^\pm$ -decay  $e^\pm$  scales linearly with  $M$  (neglecting insignificant differences due to the self-absorption). This implies that for a supermassive black hole,  $Q_{\text{s},\text{nth}}/Q_{\text{s},\text{th}}$  is larger, typically by  $\sim 2$ -3 orders of magnitude, than for  $M = 10 M_\odot$ ; see Figs 1a and 2abc. Even at  $L \simeq 0.01 L_{\text{Edd}}$ , when  $Q_{\text{s},\text{nth},\text{tot}}$  exceeds  $Q_{\text{s},\text{th},\text{tot}}$  for  $M = 10 M_\odot$  (in models with small  $\delta$ ), the stellar-mass black-hole models predict higher electron temperatures and harder X-ray spectra than supermassive black-hole models. This results from the difference of  $\nu_{\text{max}}$  noted above; for  $M = 10 M_\odot$  the seed photons are emitted mostly in the X-ray/ $\gamma$ -ray range and hence the Compton cooling is much less efficient.

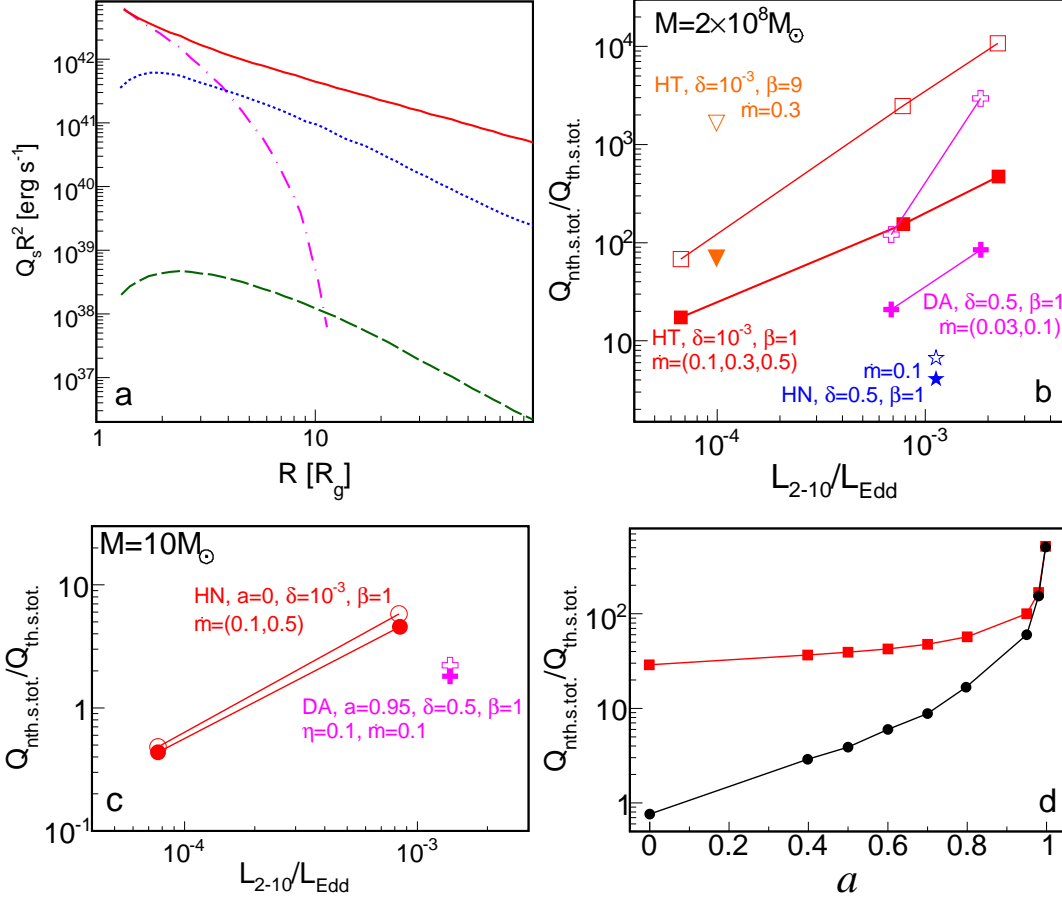


Fig. 2.— (a) Rest-frame, radial emissivity profiles for self-absorbed synchrotron radiation in models with  $a = 0.95$ ,  $\beta = 1$ ,  $\delta = 10^{-3}$  and  $\dot{m} = 0.5$ ; all  $Q_s$  rates are vertically integrated, so  $Q_s R^2$  gives the emissivity per unit volume times volume. (Blue) dotted and (green) dashed lines are for the thermal synchrotron radiation in model HT with  $M = 10 M_\odot$  (scaled by  $2 \times 10^7$ ) and  $M = 2 \times 10^8 M_\odot$ , respectively. (Red) solid and magenta (dot-dashed) lines are for the nonthermal synchrotron radiation in model HN and HT, respectively, with  $M = 2 \times 10^8 M_\odot$  (or  $M = 10 M_\odot$  with the above scaling). In panels (b) and (c), open symbols show the ratio of  $Q_{\text{nth.s.tot.}}$  to  $Q_{\text{th.s.tot.}}$ , as a function of the 2-10 keV Eddington ratio, in model DA (magenta crosses) and hadronic models (other symbols); full symbols show the ratio of the same  $Q_{\text{nth.s.tot.}}$  to  $Q_{\text{th.s.tot.}}$  in corresponding models S. Panel (b) is for  $M = 2 \times 10^8 M_\odot$ ; (red) squares: model HT with  $a = 0.98$ , (orange) triangle-down: model HT with  $a = 0.95$ ; (blue) star: model HN with  $a = 0.95$ ; (magenta) crosses: model DA with  $\eta = 0.1$  and  $a = 0.95$ ; other model parameters as specified in the figure. Panel (c) is for  $M = 10 M_\odot$ ; (red) circles: model HT, (magenta) crosses: model DA (with  $\gamma_0 = 20$ ). (d) The ratio of  $Q_{\text{nth.s.tot.}}$  in model HN (red squares), or HT (black circles), to  $Q_{\text{th.s.tot.}}$  in corresponding model S, as a function of the black hole spin parameter, for  $M = 2 \times 10^8 M_\odot$ ,  $\beta = 1$ ,  $\delta = 10^{-3}$  and  $\dot{m} = 0.3$ .

*Accretion rate.* As seen in Fig. 2b, the  $Q_{s,\text{nth,tot}}/Q_{s,\text{th,tot}}$  ratio strongly increases with increasing luminosity, as a result of (1) the decrease of the electron temperature with increasing  $\dot{m}$  (due to the increase of  $\tau$ ) leading to the decrease of  $Q_{s,\text{th,tot}}$ , and (2) the increase of  $Q_{s,\text{nth,tot}} \propto \dot{m}^2$ . Then, the difference between the hadronic and standard model also increases with  $L$ , see Fig. 1b. As also seen in Fig. 1b, the X-ray spectra harden with increasing  $L$  in both versions of the model. The hardening is due to a rather slow increase of  $\tau$  ( $\propto \dot{m}$ ) with increasing  $L$ . Namely, for heating of electrons dominated by Coulomb interactions,  $L \propto \dot{m}^\zeta$ , with  $\zeta = 2.2\text{--}2.5$  depending on the model parameters (the increase is slightly faster than  $\dot{m}^2$  due to the decrease of  $T_e$ ) and then  $\tau \propto \dot{m}^{1/\zeta}$ . The hardening is, however, much stronger in the standard model in which the flux of seed photons decreases, in contrast to the hadronic models in which it increases with increasing  $\dot{m}$ , as noted above.

*Black hole spin and proton distribution function.* The rate of pion production depends on the number of protons with energies above the pion production threshold and for the thermal distribution of protons it strongly depends on the proton temperature,  $T_p$ . In turn,  $T_p$  increases with increasing  $a$  because the rapid rotation of a black hole stabilizes the circular motion of the flow and increases the dissipation rate; for  $a = 0$ ,  $T_p$  in the innermost part is typically by a factor of  $\sim 4$  smaller than for the maximum value,  $a = 0.998$ , with other parameters unchanged. The resulting dependence of the power emitted by pion-decay electrons on  $a$  in model HT is shown in Fig. 2d; as we can see,  $Q_{s,\text{nth,tot}}/Q_{s,\text{th,tot}}$  differs by three orders of magnitude between a non-rotating and an extremely-rotating black hole. However, the dependence on  $a$  is significantly reduced in model HN, as also shown in Fig. 2d, because for a power-law distribution of protons the fraction of protons above the threshold is only linearly dependent on the average proton energy (cf. M99). For  $a \gtrsim 0.9$ , properties of the hadronic model are almost independent of the proton distribution; the pion production rate for HT and HN is almost the same in the innermost part where the dominating contribution to  $Q_{s,\text{nth,tot}}$  comes from, see Fig. 2a.

### 3.2. Directly accelerated electrons

We consider model DA for  $\delta = 0.5$ ; as noted above, for such large values of  $\delta$  the hadronic effects negligibly affect the electron temperature. In model DA the importance of self-absorption strongly depends on details of electron acceleration. If electrons are injected with a power-law distribution,  $n_{\text{inj}}(\gamma) \propto \gamma^{-s_{\text{inj}}}$ , for  $s_{\text{inj}} > 2$  most of the injected power is thermalized by self-absorption (see e.g. Malzac & Belmont 2009) and only a small fraction available as the seed photon input.

To make comparison of the hadronic model with model DA not affected by such differences, we assume an injection of nonthermal electrons with  $\gamma_0 = 100$  for  $M = 2 \times 10^8 M_\odot$ , similar as for pion-decay electrons, and  $\gamma_0 = 20$  for  $M = 10 M_\odot$  (this value is explained below). For such a monoenergetic injection, the steady state distribution of electrons is  $N(\gamma) \propto \gamma^{-2}$  and the self-absorption effects are insignificant, like in the hadronic models.

Figs 2bc illustrate effects of nonthermal electrons in model DA with  $\eta = 0.1$ , which value of  $\eta$  gives a similar  $Q_{s,\text{nth,tot}}/L$  ratio as in model HT with large  $a$  or model HN. We first note that for a large (and constant)  $\delta$ , the  $L \propto \dot{m}$  scaling implies  $\tau \propto L$ , i.e.  $\tau$  increases much faster with  $L$  than for a small  $\delta$ . As a result,  $T_e$  decreases with increasing  $L$  faster in large- $\delta$  models, leading to a stronger decrease of  $Q_{\text{th,s,tot}}$ . In model S (with large  $\delta$ ), it results in hardening of the X-ray spectra with increasing  $L$ . In model DA with  $M = 2 \times 10^8 M_\odot$ , however, the seed photon flux increases proportionally to  $L$  and this, combined with the fast increase of  $\tau$ , leads to a softening of the X-ray spectra (illustrated in Fig. 3c below).

For  $M = 10 M_\odot$ , the presence of nonthermal electrons in model DA with  $\eta = 0.1$  negligibly affects the electron temperature. Here, similarly as in hadronic models,  $Q_{\text{nth,s,tot}}$  exceeds  $Q_{\text{th,s,tot}}$  only at  $L \gtrsim 0.01 L_{\text{Edd}}$ . To check the maximum possible impact of the nonthermal synchrotron radiation at  $L \sim 0.01 L_{\text{Edd}}$ , we have assumed  $\gamma_0 \sim 20$  for which most of the nonthermal synchrotron photons are emitted at  $\sim 1$  keV (i.e. at lower energies than in the hadronic model), not much higher than  $h\nu_t$ . Even for such  $\gamma_0$ , the Compton cooling rate in Eddington units is by a factor of several smaller than in the same model DA with  $M = 2 \times 10^8 M_\odot$ ; see

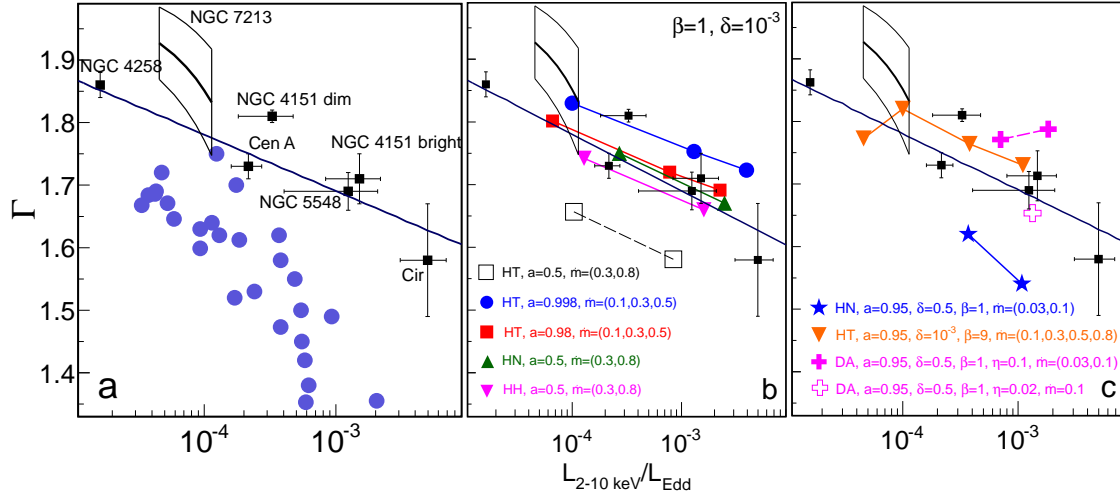


Fig. 3.— Photon spectral index as a function of the 2-10 keV Eddington ratio, predictions of the hot-flow model with  $M = 2 \times 10^8 M_\odot$  are compared with the observational data for low-luminosity AGNs (see text; dark blue line shows fit from Gu & Cao 2009). (a) The standard ADAF model S. (b) Hadronic models with  $\delta = 10^{-3}$  and  $\beta = 1$ . (c) Hadronic and DA models.

also Dermer et al. (1991) for the dependence of the cooling rate on the seed photon energy.

#### 4. Comparison with low-luminosity AGNs

In Fig. 3 we compare the  $\Gamma$ - $\lambda_{2-10}$  (where  $\lambda_{2-10} = L_{2-10}/L_{\text{Edd}}$ ) relation predicted in our model with the observational data for low-luminosity AGNs, same as used in N14. The sample includes nearby AGNs with precisely measured black-hole masses and the spectra measured with high-quality statistics, which allows to estimate the intrinsic X-ray spectrum. The values of the intrinsic  $\Gamma$  and  $L_{2-10}$  are taken from Lubiński et al. (2010) for the dim and bright states of NGC 4151, Brenneman et al. (2012) for NGC 5548, Beckmann et al. (2011) for Centaurus A, Yamada et al. (2009) for NGC 4258 and Yang et al. (2009) for Circinus; see N14 for details. To find  $\lambda_{2-10}$  we use black-hole mass measurements quoted in N14, except for NGC 4151 for which we use the new stellar dynamical mass measurement,  $M = (3.76 \pm 1.15) \times 10^7 M_\odot$  (Onken et al. 2014). We also use fits to the  $\Gamma$ - $\lambda_{2-10}$  anticorrelation in a large sample of low-luminosity AGNs from Gu & Cao (2009) and in NGC 7213 from Emmanoulopoulos et al. (2012).

Fig. 3a shows the model points for model S,

including all results for models with  $M = 2 \times 10^8 M_\odot$  from N14 and several additional solutions for model S corresponding to hadronic models computed in this work. The clear discrepancy between the model and the data was noted in Section 1 as a motivation for this work. The two model points located close to Cen A are for the models (with  $\delta = 0.5$ ) with very tenuous flows, having  $\tau \lesssim 0.01$  and  $kT_e \gtrsim 1$  MeV; extension of this model to lower  $L$  can approximately reproduce the relation assessed in NGC 7213 if the average slope of the X-ray spectrum is considered, however, these X-ray spectra strongly deviate from a power-law.

As we can see in Fig. 3b, the hadronic model with small  $\delta$  reproduces the  $\Gamma$ - $\lambda_{2-10}$  relation observed in AGNs. Model HN agrees with the AGN data regardless of the black-hole spin value; note also that model HH gives a similar  $\Gamma$ - $\lambda_{2-10}$  relation to model HN, so it is not very sensitive to the fraction of total energy in the nonthermal proton component. Model HT agrees with the data for large values of  $a$ ; for  $a \lesssim 0.9$  it predicts slightly too hard spectra, e.g. by  $\Delta\Gamma \simeq -0.1$  for  $a = 0.5$ .

The model solutions shown in Fig. 3b correspond to  $\beta = 1$ . As we see in Fig. 3c, the hadronic model with  $\beta = 9$  gives a similar relation, except for the lowest  $\lambda_{2-10}$  for which the compressive



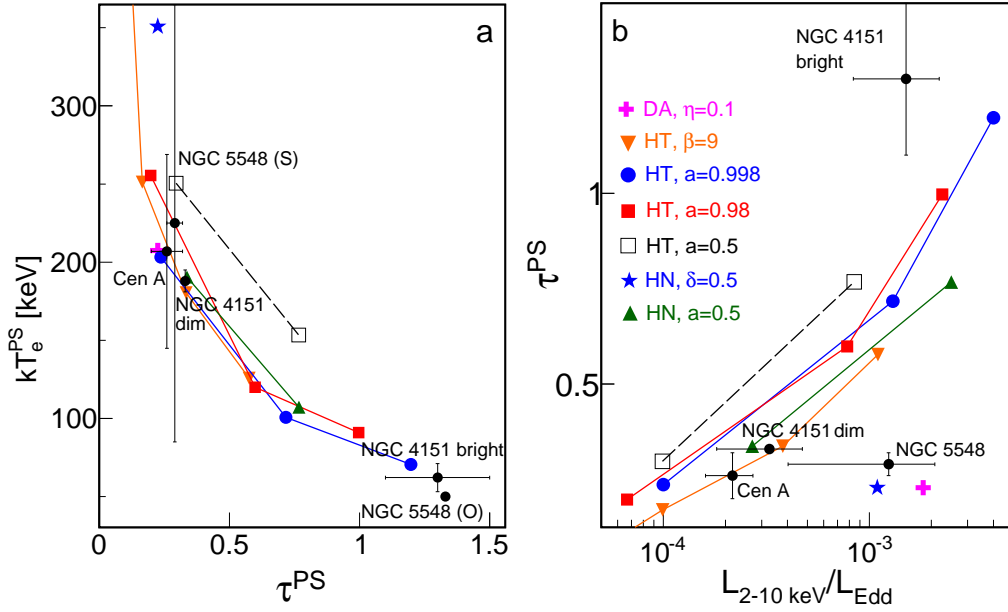


Fig. 4.— (a)  $T_e^{\text{PS}}$  as a function of  $\tau^{\text{PS}}$ , (b)  $\tau^{\text{PS}}$  as a function of  $\lambda_{2-10}$ ; parameters of the COMPPS slab model best-matching the hot-flow spectra compared with plasma parameters measured in several AGNs (see text). In both panels: (blue) circles are for model HT with  $a = 0.998$ ,  $\delta = 10^{-3}$ ,  $\beta = 1$ ,  $\dot{m} = 0.1, 0.3$  and  $0.5$ ; (red) squares are for model HT with  $a = 0.98$ ,  $\delta = 10^{-3}$ ,  $\beta = 1$ ,  $\dot{m} = 0.1, 0.3$  and  $0.5$ ; (green) triangles-up are for model HN with  $a = 0.5$ ,  $\delta = 10^{-3}$ ,  $\beta = 1$ ,  $\dot{m} = 0.3$  and  $0.8$ ; (black) open squares are for model HT with  $a = 0.5$ ,  $\delta = 10^{-3}$ ,  $\beta = 1$ ,  $\dot{m} = 0.3$  and  $0.8$ ; (orange) triangles-down are for model HT with  $a = 0.95$ ,  $\beta = 9$ ,  $\delta = 10^{-3}$ ,  $\dot{m} = 0.1, 0.3, 0.5$  and  $0.8$ ; (blue) star is for model HN with  $\beta = 1$ ,  $\delta = 0.5$ ,  $\dot{m} = 0.1$ ; (magenta) cross is for model DA with  $a = 0.95$ ,  $\delta = 0.5$ ,  $\dot{m} = 0.1$  and  $\eta = 0.1$ .

heating of electrons dominates, leading to  $\tau \propto L$ , and then in this range we get a positive correlation (similarly as in model DA, see below). Stars in Fig. 3c are for the hadronic model with  $\delta = 0.5$ , which differs only weakly from model S as discussed in Section 3.1.

Dashed line in Fig. 3c illustrates the positive  $\Gamma$ - $\lambda_{2-10}$  correlation in model DA with a constant  $\eta = 0.1$  which, as noted in Section 3.2, results from (1) the linear increase of  $\tau$  with  $L$ , combined with (2) the linear increase of seed photon flux with  $L$ . The model with  $\eta \sim 0.1$  can explain the intrinsic X-ray slopes measured in AGNs. However, the decrease of  $\eta$  is required (if  $\delta$  does not decrease significantly with increasing  $\dot{m}$ ), by a factor of  $\sim 2$  for the increase of  $L$  by a factor of 3, to reproduce the observed negative relation.

Finally, we note that the slope of the  $\Gamma$ - $\lambda_{2-10}$  correlation observed in individual AGNs, NGC 4151 (the change between dim and bright states) and NGC 7213, is slightly steeper than predicted by the hadronic models. Then, an additional, weak contribution of directly accelerated electrons may be required at lower  $\dot{m}$ .

Further constraints on physics of hot flows can be obtained by modeling of the observed spectra with thermal Comptonization model. It allows to estimate the electron temperature, which is directly related to the cut-off energy, and the optical depth, which in combination the temperature determines the slope of the spectrum. However, precise measurements of the high-energy cut off are necessary for such modeling, which is a challenging task for AGNs due to poor quality of the hard X-ray data. Such measurements are available only for a few brightest AGNs, furthermore, there is a discrepancy in results based on data provided by different detectors (see e.g. discussion in Lubiński et al. 2010).

Similarly as in N14, we have fitted the hot flow spectra using the slab COMPPS model (Poutanen & Svensson 1998). The fitted parameters,  $T_e^{\text{PS}}$  and  $\tau^{\text{PS}}$ , are compared in Fig. 4 with plasma parameters assessed in AGNs with relevant  $\lambda_{2-10}$ . We use the COMPPS fits for NGC 4151 (Lubiński et al. 2010), Cen A (Beckmann et al. 2011) and NGC 5548 (Brenneman et al. 2012). In Fig. 4a we plot also the thermal Comptonization fit for NGC 5548 from Magdziarz et al. (1998). The parameters from Brenneman et al. (2012) and Magdziarz

et al. (1998) are denoted by S (*Suzaku*) and O (OSSE), respectively; their fits used the sphere models, so we use the fitted  $\tau$  reduced by a factor of 2 and 1.5, respectively, which reduction factors correspond to the fitted values of  $\tau$  (see N14).

As we see, various hadronic models with small  $\delta$  (except for model HT with small or moderate  $a$ ) predict similar  $T_e^{\text{PS}}(\tau^{\text{PS}})$  relations, which are in agreement with plasma parameters measured in AGNs. Similarly, model DA with  $\eta = 0.1$  agrees with the AGN data at  $\tau^{\text{PS}} \simeq 0.2$ . In N14 we found that lower values of  $\beta$  give lower  $T_e^{\text{PS}}$  through the change of the flow geometry. Namely, lower- $\beta$  flows are closer to a slab and higher- $\beta$  flows are closer to a sphere and, thus, the Compton cooling is less efficient in the latter. In the hadronic models, however, the dependence of the  $T_e^{\text{PS}}(\tau^{\text{PS}})$  relation on  $\beta$  is reduced; the large- $\beta$  flows have much larger proton temperatures and the larger pion-production rate approximately compensates the difference in geometry.

Larger differences between the model predictions, especially those for high and low values of  $\delta$ , occur in the  $\tau^{\text{PS}}(\lambda_{2-10})$  relation (Fig. 4b). At  $\lambda_{2-10} \sim 10^{-3}$ ,  $\delta = 0.5$  gives  $\tau^{\text{PS}}$  by a factor of several lower than  $\delta = 10^{-3}$ . As we see, values of  $\tau^{\text{PS}}$  estimated in NGC 4151 and Cen A strongly favor low values of  $\delta$ . In turn,  $\tau^{\text{PS}}$  estimated from the *Suzaku* data of NGC 5548 is consistent with large  $\delta$ . However, we emphasize again that the estimation of  $\tau^{\text{PS}}$  strongly relies on the precise determination of the spectral cut-off and the discrepancies between different studies of the observed data, noted above, are similar in magnitude to the differences in the model predictions. The observational uncertainty is illustrated by the difference between plasma parameters for NGC 5548 obtained using the *Suzaku* and OSSE data; almost the same difference for the bright state of NGC 4151 follows from studies of the *Integral* data by Lubiński et al. (2010) and *BeppoSAX* data by Petrucci et al. (2001).

## 5. Summary and discussion

The  $\Gamma$ - $\lambda_{2-10}$  relation, which can be robustly determined in nearby AGNs, indicates that a source of seed photons much stronger than thermal synchrotron is needed to explain the X-ray radiation of low-luminosity AGNs by thermal Comp-

tonization in hot accretion flows. Using a precise hot-flow model we find that the nonthermal synchrotron emission of relativistic electrons is a good candidate for a sufficiently efficient source. If the power in the nonthermal electron component equals  $\sim 10$  per cent of the power used to heat the thermal electrons, the model can explain the observed relation essentially for any value of  $a$ ,  $\beta$  or  $\delta$ . The origin of the non-thermal component with such a magnitude can be explained by two different mechanisms and it depends on the value of  $\delta$ .

If thermal electrons are heated mainly by Coulomb interactions (low  $\delta$ ), the nonthermal electrons may come from the decay of pions produced by proton-proton interactions. The flux of nonthermal synchrotron photons is then determined by the hydrodynamic solution and the proton distribution function. Remarkably, the hadronic collisions produce a sufficient amount of nonthermal electrons for a broad range of parameters, excluding only a moderately or slowly rotating black hole with a thermal distribution of protons. The idea that relativistic protons may be responsible for the production of relativistic electrons was considered in several works in 1980s (e.g. Kazanas & Ellison 1986, Zdziarski 1986, Sikora et al. 1987), following realization that the direct Fermi acceleration of electrons is much less efficient than the acceleration of protons and, thus, electrons produced by pion decay should outnumber those directly accelerated.

If a large fraction of the accretion power is used for the direct heating of thermal electrons (large  $\delta$ ), the nonthermal component must be due to direct acceleration of electrons. Such acceleration of electrons is indeed possible in hot flows according to recent MHD simulations (e.g. Ding et al. 2010, Riquelme et al. 2012). In this version of the model, a specific scaling of the thermal heating and acceleration parameters,  $\delta$  and  $\eta$ , with the accretion rate is needed to explain the observed  $\Gamma$ - $\lambda_{2-10}$  anticorrelation. We note that although  $\delta$  and  $\eta$  are treated as independent parameters in our computations, they are certainly related to the same microphysical processes that convert the accretion power into the plasma kinetic energy. We also emphasize that a value of  $\eta \sim 0.1$ , sufficient to explain the observed data, was assessed under the assumption of monoenergetic injection of elec-

trons. A more realistic scenario, with electrons accelerated into a power-law distribution with the index  $s_{\text{inj}}$ , is properly approximated by the monoenergetic injection only for  $s_{\text{inj}} < 2$ . For larger  $s_{\text{inj}}$  (which are supported by some observations, see below), a significant fraction of nonthermal energy is self-absorbed (for  $s_{\text{inj}} \gtrsim 3.5$  this may be the only form of thermal plasma heating, cf. Malzac & Belmont 2009) and then a larger value of  $\eta$  would be required.

The plasma parameters predicted by the large- $\delta$  and small- $\delta$  models differ significantly and a precise estimation of the electron temperature and optical depth should allow to constrain the value of  $\delta$ . However, results provided by different detectors disagree even for brightest AGNs. Results of some studies (based on OSSE or *Integral* data) seem to favor low values of  $\delta$ , while other (using *BeppoSAX* or *Suzaku* data) appear more consistent with large  $\delta$ .

In flows surrounding stellar-mass black holes, the nonthermal synchrotron is emitted in the X-ray/ $\gamma$ -ray range. Therefore, the Compton cooling is much weaker, and the presence of the nonthermal electron component receiving  $\sim 10$  per cent of the total power (due to pion-decay for small  $\delta$  or direct acceleration for large  $\delta$ , similarly is in AGN models) insignificantly affects the electron temperature. The X-ray spectra predicted by both the hadronic and direct acceleration models for  $M = 10 M_{\odot}$  differ only weakly from the spectra predicted by the standard model (with the thermal synchrotron only), which were studied in detail in N14. In N14 we found that the evolution of black-hole transients agrees with predictions of the standard model, in particular they reach  $\Gamma \simeq 1.4$  at  $L \sim 0.01 L_{\text{Edd}}$  (as compared to the intrinsic  $\Gamma \gtrsim 1.7$  measured in AGNs at such  $L$ ). The results of this work indicate that the agreement does not exclude the presence of a significant nonthermal electron component.

We conclude that the hot flow model with seed photons produced by the nonthermal synchrotron radiation provides an attractive description for all accreting black-hole systems, with the difference between AGNs and black-hole transients around  $\sim 0.01 L_{\text{Edd}}$  explained by the scaling of basic physical processes with the black-hole mass.

Finally, we comment on the observability of spectral features formed by pion-decay  $e^{\pm}$ . The

annihilation feature is not observable, e.g. for the model shown in Fig. 1(c) the observed luminosity of the annihilation photons is  $\sim 10^{33}$  erg/s. The high-energy part of the synchrotron radiation perhaps could be observed in bright nearby objects, like Cyg X-1. However, the MeV tail which is observed in Cyg X-1 at  $L \simeq 0.01L_{\text{Edd}}$  (e.g. Del Santo et al. 2013) is over an order of magnitude stronger than the synchrotron component predicted by the model, as shown in Fig. 1(c) for the solution with  $L \simeq 0.007L_{\text{Edd}}$ . If the observed tail is produced in the hot flow, it indicates that an efficient direct acceleration must take place in the flow, because the  $\pi^\pm$ -decay electrons cannot produce a tail with such a magnitude at such  $L$ . However, the tail may be produced in other sites, e.g. in a cold disc corona, as suggested e.g. by the increase of the relative strength of the nonthermal component with the increasing intensity of the thermal disc emission, assessed by Del Santo et al. (2013). We note also that the high-energy tail in GX 339-4 was revealed in the rising phase of GX 339-4 by Droulans et al. (2010) at  $L/L_{\text{Edd}}$  much larger than these of our solutions and the results of this work cannot be used to estimate the corresponding strength of pion-decay component. A relevant hot flow model, with strong Coulomb cooling of protons, would be characterized by a much larger density and hence, for a nonthermal proton distribution, by an enhanced pion production.

Interestingly, spectral modeling of the above observations of nonthermal tails with hybrid models indicate that a steep injection index of electrons,  $s_{\text{inj}} \gtrsim 2.5$ , is required. Such a steep injection can be explained by the decay of pions for a steep acceleration index of protons, such as assumed in our computations.

We thank the referee for useful comments. This research has been supported in part by the Polish NCN grant N N203 582240. FGX is supported by the National Basic Research Program of China (973 Program, grant 2014CB845800), the NSFC (grants 11203057, 11103061, 11133005 and 11121062), and the Strategic Priority Research Program "The Emergence of Cosmological Structures" of the Chinese Academy of Sciences (Grant XDB09000000).

## REFERENCES

- Beckmann V., Jean P., Lubiński P., Soldi S., Terrier R., 2011, AA, 531, 70
- Brenneman L., Elvis M., Krongold Y., Liu Y., Mathur S., 2012, ApJ, 744, 13
- Del Santo, M., Malzac, J., Belmont, R., Bouchet, L., & De Cesare, G. 2013, MNRAS, 430, 209
- Dermer, C. D., Liang, E. P., Canfield, E., 1991, ApJ, 369, 410
- Ding, J., Yuan, F., & Liang, E. 2010, ApJ, 708, 1545
- Done, C., Gierliński, M., & Kubota, A. 2007, A&A Rev., 15, 1
- Droulans, R., Belmont, R., Malzac, J., & Jourdain, E. 2010, ApJ, 717, 1022
- Emmanoulopoulos, D., Papadakis, I. E., McHardy, I. M., et al. 2012, MNRAS, 424, 1327
- Ghisellini, G., & Svensson, R. 1991, MNRAS, 252, 313
- Gu M., Cao X. 2009, MNRAS, 399, 349
- Kazanas, D., & Ellison, D. C. 1986, ApJ, 304, 178
- Kimura, S. S., Toma, K., & Takahara, F. 2014, ApJ, 791, 100
- Lubiński, P., Zdziarski, A. A., Walter, R., et al. 2010, MNRAS, 408, 1851
- Magdziarz, P., Blaes, O. M., Zdziarski, A. A., Johnson, W. N., & Smith, D. A. 1998, MNRAS, 301, 179
- Mahadevan R. 1997, ApJ, 477, 585
- Mahadevan R. 1999, MNRAS, 304, 501 (M99)
- Malzac J., Belmont R. 2009, MNRAS, 392, 570
- Manmoto T., 2000, ApJ, 534, 734
- Moskalenko, I. V., & Strong, A. W. 1998, ApJ, 493, 694
- Narayan, R., & Yi, I. 1995, ApJ, 452, 710

- Niedźwiecki, A., Xie, F.-G., Zdziarski, A. A. 2012, MNRAS, 420, 1195 (N12)
- Niedźwiecki, A., Xie, F.-G., & Stępnik, A. 2013, MNRAS, 432, 1576 (N13)
- Niedźwiecki, A., Xie, F.-G., & Stępnik, A. 2014, MNRAS, 443, 1733 (N14)
- Onken, C. A., Valluri, M., Brown, J. S., et al. 2014, ApJ, 791, 37
- Petrucci P. O., et al., 2001, ApJ, 556, 716
- Poutanen, J., Svensson, R. 1996, ApJ, 470, 249
- Poutanen, J., & Veledina, A. 2014, Space Sci. Rev., 183, 61
- Riquelme, M. A., Quataert, E., Sharma, P., & Spitkovsky, A. 2012, ApJ, 755, 50
- Sikora, M., Kirk, J. G., Begelman, M. C., & Schneider, P. 1987, ApJ, 320, L81
- Veledina A., Vurm I., Poutanen J. 2011, MNRAS, 414, 3330
- Wardziński, G., & Zdziarski, A. A. 2001, MNRAS, 325, 963
- Xie F.-G., Niedźwiecki A., Zdziarski A. A., Yuan F., 2010, MNRAS, 403, 170
- Yamada S., Itoh T., Makishima K., Nakazawa K. 2009, PASJ, 61, 309
- Yang Y., Wilson A. S., Matt G., Terashima Y., Greenhill L. J., 2009, ApJ, 691, 131
- Yuan, F., & Narayan, R. 2014, ARA&A, 52, 529
- Yuan, F., Xie, F., & Ostriker, J. P. 2009, ApJ, 691, 98
- Zdziarski, A. A. 1986, ApJ, 305, 45
- Zdziarski A. A., Gierliński M. 2004, Progress Theor. Phys. Suppl., 155, 99